Chapter 5

Porous Ceramic Composite using Industrial Solid Waste (Coal Overburden) via Alumina Dissolution Process

5.1 Introduction

The preceding chapters have effectively fulfilled the primary objective of this thesis, introducing innovative, straightforward, and cost-effective techniques for fabricating porous ceramics and foams. The subsequent chapters will focus on addressing the secondary objective of this work, which involves fabricating porous composites derived from waste materials and conducting thermomechanical characterization. By accomplishing this objective, the overarching goal of "Waste Valorization" will be achieved, whereby waste materials are utilized in a valuable and sustainable manner.

Literature search has shown many attempts in utilizing solid wastes (including solid waste with higher content of Alumina) from lab scale to market scale. In Section 2.5 of Chapter 2, a comprehensive list of waste materials such as fly ash, steel slag, mine tailings, and red mud, among others, is provided. The section explores various methods and techniques employed to convert these waste materials into valuable products. However, these attempts either lacks economic feasibility or lack mass conversion productivity. Thus, effective utilization of these solid wastes remains as challenge. Therefore, the present investigation is first of its kind, wherein an attempt has been made to utilize a facile but economical feasible porous fabrication technique to utilize solid waste having alumina as its content to make high strength and highly porous composite successfully which can be effectively used for mass conversion of these wastes. The proposed procedure is based on Alumina dissolution process in an acidic media. The present process is economically viable and easy adaptable with minimum resource for processing porous composites. Coal mine overburden waste has been used in present study as model waste.

The present chapter elucidates the efficient utilization of the "Alumina dissolution process" to convert "Coal overburden waste" into highly porous aluminosilicate-based composites (PAC). The chapter also investigates the suitability of these porous composite for insulation applications through thermo-mechanical characterization. The flexible porosity range with high strength give this procedure an extra edge to be used for various applications, thus present technique gives way a for mass conversion of such wastes. The high-temperature heat treatment involved in the sintering process of the porous composites not only consolidates and strengthens the porous structure but also facilitates the formation of various aluminosilicate phases incorporating heavy metals such as spinel, albite, and anthracite. This ultimately contributes to the mitigation of heavy metal contaminants present in the raw solid waste. It is anticipated that the outcomes of this study will inspire researchers and industrialists to embrace

this novel and cost-effective technique for successfully converting hazardous solid waste, particularly those containing alumina, into valuable porous composites. Considering the economic and environmental benefits associated with the utilization of such waste materials, this approach holds significant promise.

5.2 Materials and Method

5.2.1 Raw Materials

MW collected from the Bina site, NCL Singrauli, India, serves as the primary ingredient for PAC fabrication. The collected MW samples undergo air-drying, grinding, and sieving through a 180-micron sieve. Concentrated H_2SO_4 (98 wt.%) of laboratory research quality from Loba, India, is utilized in the experiment.

5.2.2 Fabrication Methodology

The fabrication process of PAC is based on the alumina dissolution process, utilizing the alumina content present in MW as the precursor material for porous fabrication. Initially, sieved MW samples are combined with deionised (DI)water in a specified concentration, resulting in a slurry paste. This slurry is cast into a suitable mold and optimized quantity of sulphuric acid is then added to the slurry. The mold is then placed in a pre-heated oven at 100°C for 24 hours to allow for reaction and foaming. The foamed samples are subsequently dried in an oven at 100°C. The dried green foam samples are machined to achieve the desired shape and then subjected to the sintering process at temperatures ranging from 1400°C to 1500°C, promoting final foaming and consolidation. For simplicity, only three solid loadings (65%, 70%, and 75%) are considered based on previous experiments. The fabrication process and detailed methodology can be found in Chapter 3. Figure 5.1 provides a schematic representation of the fabrication process employed to produce PAC.

5.2.3 Characterization Techniques

To assess the quantitative and qualitative characteristics of raw MW, a series of physicochemical characterizations were performed. The particle size distribution of MW was determined using Dynamic Light Scattering technology (Malvern). The presence of various oxides in raw MW was analyzed using X-ray Fluorescence (XRF) spectroscopy (S8 Tiger, Bruker model). X-ray diffraction (XRD) measurements of both raw MW and sintered PAC were conducted on a Rigaku Miniflex 600 Desktop X-Ray Diffractometer, using Cu-kα (1.54 Å) radiation within a 2θ range of 5-80° with a step size of 0.02°.

To understand the surface morphology and microstructure of raw MW and PAC, scanning electron microscopy (SEM) was performed using an EVO-MA15/18 microscope from Carl Zeiss Microscopy Ltd. Fourier-transform infrared spectroscopy (FTIR) analysis (Nicolet iS5; Thermo Electron Scientific Instruments LLC) was employed to observe changes in functionality and bonds during the pre- and post-dissolution process, as well as during sintering.

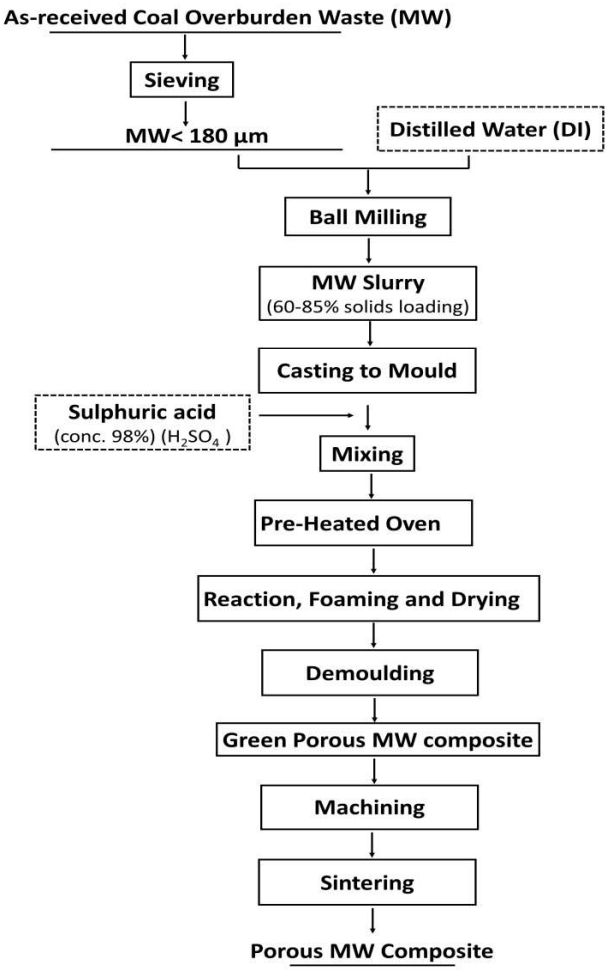

Fig. 5.1 Fabrication process of PAC

Thermogravimetric analysis (TGA) was carried out using a TGA-50 instrument from Shimadzu (Asia Pacific) Pte Ltd to determine the thermal decomposition behavior of green PAC. The open porosity of the samples was determined using the Archimedes' displacement method based on water immersion, while bulk density and total porosity were calculated using established test procedures. The following formulas were utilized for the calculations:

$$BD = \frac{m}{V} \quad (1)$$

$$TP = \left(1 - \frac{BD}{\gamma}\right) \times 100 \quad (2)$$

$$OP = \left(\frac{w-m}{w-s}\right) \times 100 \quad (3)$$

where, BD is the bulk density of the sample in grams per cubic centimetre, m is the dry weight of the composite in grams, V is the volume of the prepared composite, TP is the total porosity of the foam, γ is the density of MW powder, OP is the open porosity of the sample, w is the soaked weight measured after soaking the composite in water for 24 hours, and s is the suspended weight of the sample. For compression testing, compressive samples were rigorously produced following the ASTM C1161-18 standard, and they were tested on a Universal Testing Machine (INSTRON) with a crosshead speed of 0.2 mm/min. PAC cuboids with dimensions of 30 by 12 by 12 mm were fabricated for the compression tests. The thermal conductivity of the PAC was measured using Hot Disk equipment (TPS-500, Goteborg, Sweden).

5.3 Results and Discussion

5.3.1 Characterization of Raw MW

The Initial observation of the ungrounded and non-sieved raw MW indicates a mixture of fragmented fine- and coarse-grained sandstone, shale, soft clay and carbonaceous shale. Initially, MW was grounded and sieved using the ball-milling technique to get uniform and finer powder (Fig. 5.2(a)). It was envisaged with the help of DLS technique and SEM micrograph that MW powder presents a fine and uniform particle size distribution with an average particle size of 1.194 μm (Fig. 5.2(b, c)). BET analysis reveals that these MW particles exhibit a surface area of 4.74 m^2/g and a mean pore diameter of 34.61nm. MW is found to be acidic in nature, having a pH of 6.2 as measured using a digital pH meter. Elemental analysis using EDX confirms the presence of Al, Si, O, Fe, Ti, Mn, Mg, P, Ca, K, Na elements in raw MW (Fig. 5.2(d)). Chemical composition of MW was identified and quantified using XRF, which reveals the presence of high fractions of Silica and Alumina with a lower fraction of oxides of Iron, Titanium, Potassium, Magnesium, Sodium and Calcium (Table 5.1). The majority of the minerals found in MW samples include quartz, tridymite, aluminium oxide, kyanite, orthoclase, anatase, albite, titanium, sodium sulphate, magnesium sulphate, lazurite, iron sulphide, sodium aluminium, and silicate sulphur, as demonstrated by the available data (Fig. 5.3). Quartz is observed to be the dominant mineral present in the MW powder. FTIR (Fig. 5.4) analysis also corroborates the XRD observations, showing the presence of

aluminosilicate minerals in the raw MW. The two peaks observed in the range 3600-3700 cm^{-1} are due to the stretching vibration of OH group and may be attributed to Montmorillonite or Kaolinite [85]. The peak at 1040 cm^{-1} can be attributed to C-O stretching bands. A single strong peak at 1115.6 is due to the vibration of Si-O, indicating the presence of quartz. The remaining peaks in between the range of 500-1000 cm^{-1} can be ascribed to the stretching bands of Si-O, C-C, and OH and can be attributed to the presence of Silica and carbon. The observed peaks well matched with the peaks available in the literature, confirming the existence of these minerals in the raw MW sample [64,81,144].

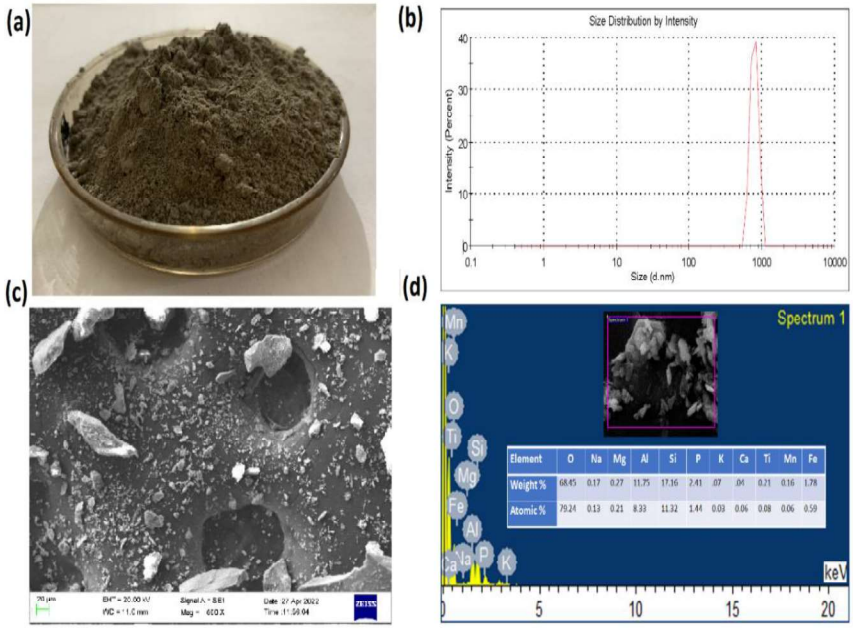

Fig. 5.2 (a) Milled and sieved raw MW, (b) Particle size distribution (c) SEM image, (d) EDX analysis, of sieved raw MW powder

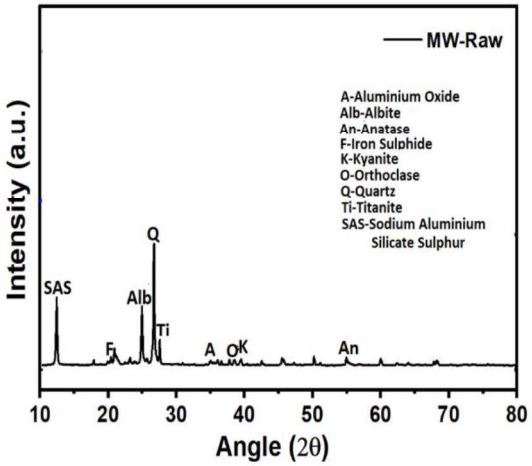

Fig. 5.3 XRD analysis of raw MW

Table 5.1 Physical, chemical, and mineralogical compositions of Coal Mine Overburden Waste (MW)

Physical properties	
BET surface area	4.74 m^2/g
Mean pore diameter	34.61nm
Average particle size (DLS)	1194 nm
pH	6.2

XRF Results		**TCLP Results**	
Major oxides	***wt.%***	**Trace elements**	***ppm***
SiO_2	49.40	Cr	54.71
Al_2O_3	24.81	Co	15.94
Fe_2O_3	3.44	Pb	8.04
K_2O	2.46	Zr	196.45
MgO	1.76	Ba	272.51
Na_2O	1.07	Ni	28.46
TiO_2	1.10	Cu	29.34
CaO	1.00	V	115.25
BaO	0.17	Zn	17.34
P_2O_5	0.17	Sc	8.32
ZrO_2	0.02	Y	16.38
MnO	0.05	Sr	66.21
V_2O_5	0.03	Ce	88.1
Cr_2O_3	0.01		
CuO	0.01		
ZrO_2	0.01		
LOI	14.49		

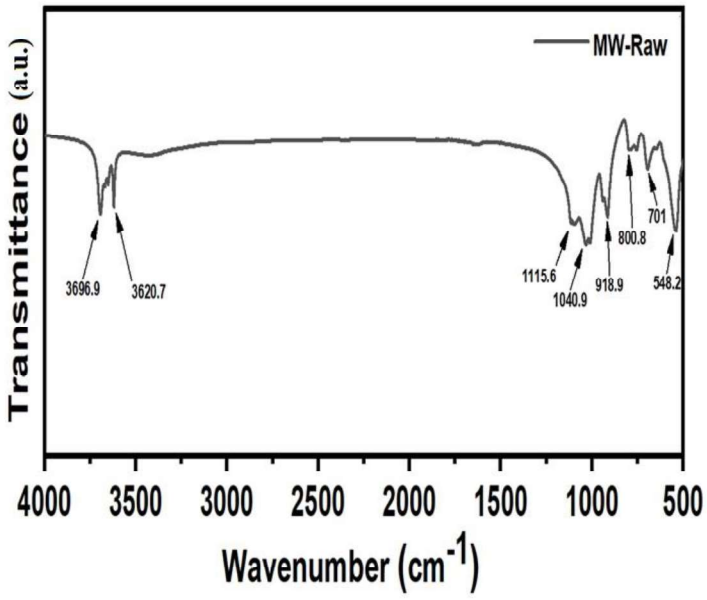

Fig. 5.4 FTIR analysis of raw MW

5.3.2 Synthesis Mechanism and Characterization of Porous Aluminosilicate Composite (PAC)

The Porous aluminosilicate composite is developed through a procedure involving the dissolution of alumina in acidic media[152]. In brief, when MW slurry is mixed with concentrated H_2SO_4, the dissolution process of alumina present in MW initiates and accelerates under heating conditions. The process begins with the hydration of alumina in acidified water, forming aluminium hydroxide. This is followed by the adsorption of hydrogen ions on the surface of the produced aluminium hydroxide, resulting in a positively charged surface of $Al(OH)^{2+}$. Eventually, the dissolution reaction concludes with the formation of both AlOOH and $[Al(OH)_2]_2SO_4$, which remain on the alumina surface. These compounds are not easily soluble in the acidic solution and hinder the dissolution process. With subsequent reactions, more of these compounds accumulate on the alumina surface, further impeding the dissolution process. It is also anticipated that presence of small amount of oxides of iron, titanium, potassium and magnesium also undergoes reaction when MW slurry added with sulphuric acid. However, due to smaller content of these oxides in MW, it can be inferred that the reaction and reaction products does not have any significance impact on foaming behaviour. The current procedure includes the dissolution of alumina, along with the simultaneous partial reactions of iron, titanium, potassium, and magnesium oxides with sulphuric acid. When magnesium oxide is dissolved in dilute sulphuric acid, it forms colourless aqueous solution of Magnesium Sulphate. This aqueous solution when evaporates and crystallizes, colourless crystals of Epsom salt are obtained. K_2O is a base and H_2SO_4 is an acid. Hence, acid-base neutralization reaction takes place. This is a type of double replacement (double displacement) reaction called a neutralization reaction. An acid and a base react to form an aqueous salt and water. Iron reacts with dilute sulphuric acid to form iron sulphate.

These reactions are hypothesized to occur as described below:

$$MW\ [Al_2O_3 + SiO_2 + Fe_2O_3 + TiO_2 + K_2O + MgO] + DI\ [H_2O] \rightarrow MW\ slurry \quad \ldots\ldots\ldots\ldots (1)$$

$$MW\ slurry + H_2SO_4 + Heat\ (100°C) \rightarrow MW + AlOOH + [Al(OH)_2]_2SO_4 + X \quad \ldots\ldots\ldots\ldots (2)$$

where $X = MgSO_4 + K_2SO_4 + Ti(SO_4)_2 + FeSO_4 + Fe_2(SO_4)_3 + SiO_2$

Al_2O_3 (aq) + H_2SO_4 (aq) → Al_2O_3 + AlOOH + $[Al(OH)_2]_2SO_4$ + H_2O (l)……..(3)

MgO (aq) + H_2SO_4 (aq) → $MgSO_4$ + H_2O (l)……..(4)

K_2O (aq) + H_2SO_4 (aq) → K_2SO_4 (aq) + H_2O (l)…… (5)

TiO (aq) +$2H_2SO_4$ (aq) → $Ti(SO_4)_2$ (aq) + $2H_2O$ (l)……..…(6)

Fe_3O_4 (aq) + $4H_2SO_4$ (aq) → $FeSO_4$+ $Fe_2(SO_4)_3$ + $4H_2O$ (l)……(7)

During the process of alumina dissolution, which leads to the formation of AlOOH and $[Al(OH)_2]_2SO_4$, the MW slurry system also experiences the generation of pores. These initial pores are formed by the presence of water bubbles, which arise due to the elevated temperature in the oven exceeding the boiling point of water. As these water bubbles transform into water vapor, they create voids within the MW slurry. The MW particles (mostly silica and unreacted alumina) surround and encapsulate these water bubbles, preventing their collapse and fusion through a particle-stabilization mechanism. This mechanism is facilitated by the formation of aluminum sulfates, which strengthen the bonding between MW particles. Once the water has completely evaporated, the resulting dried green MW composite contains pores. This body is then allowed to cool in ambient conditions before the green samples are removed from their molds. The entire drying process can take up to 12 hours. To promote further foaming and consolidation, a heat treatment is carried out on the green porous MW composite. During this heat treatment at higher temperatures, the foaming mechanism takes place, primarily driven by the decomposition of products generated during the alumina dissolution process. These products decompose at specific temperature ranges, leading to the release of gaseous by-products. The formation of pores within the structure of the green MW composite occurs as a result of these by-products, contributing to the development of secondary fine pores. The major by-products of the alumina dissolution process, namely AlOOH and $[Al(OH)_2]_2SO_4$, play a significant role in generating pores through their decomposition. On the other hand, by-products such as sulphates of Mg, K, Ti, and Fe also decompose during the thermal treatment, but their contribution to pore formation is relatively minor due to their lower quantities in the composition.

To gain a better understanding of the synthesis mechanism and changes occurred during dissolution reaction process and after sintering process in green MW composite and sintered PAC, various characterizations such as TGA, FT-IR, Raman and XRD have been utilized. The TGA analysis of the green porous MW composite provided valuable insights into the weight loss stages and corresponding temperature ranges during the heat treatment process. The TGA

curve, as shown in Fig. 5.5, exhibited three distinct stages of weight loss. The initial stage of weight loss (6.21%) occurred in the temperature range of 26-200°C and was attributed to the removal of physically adsorbed water. This stage involved the release of water molecules that were weakly bound to the surface of the MW particles. The second stage of weight loss is in continuous with first stage, and occurs in the temperature interval of 212-416°C. This stage accounted for the decomposition of aluminium hydroxide. Between 416°C and 457°C, the weight loss was negligible, with no significant change in weight observed. This period indicated a relatively stable phase during the heat treatment process. The major weight loss occurred between 457°C and 781°C, corresponding to a weight loss of approximately 6.25%. This weight loss stage was associated with the thermal decomposition of aluminium sulphate. Based on the TGA analysis, it can be inferred that the hydroxylation of MW leads to the formation of aluminium hydroxide and aluminium sulphate as major products. These compounds subsequently decompose at higher temperatures during the heat treatment process, resulting in the creation of secondary pores within the green MW samples.

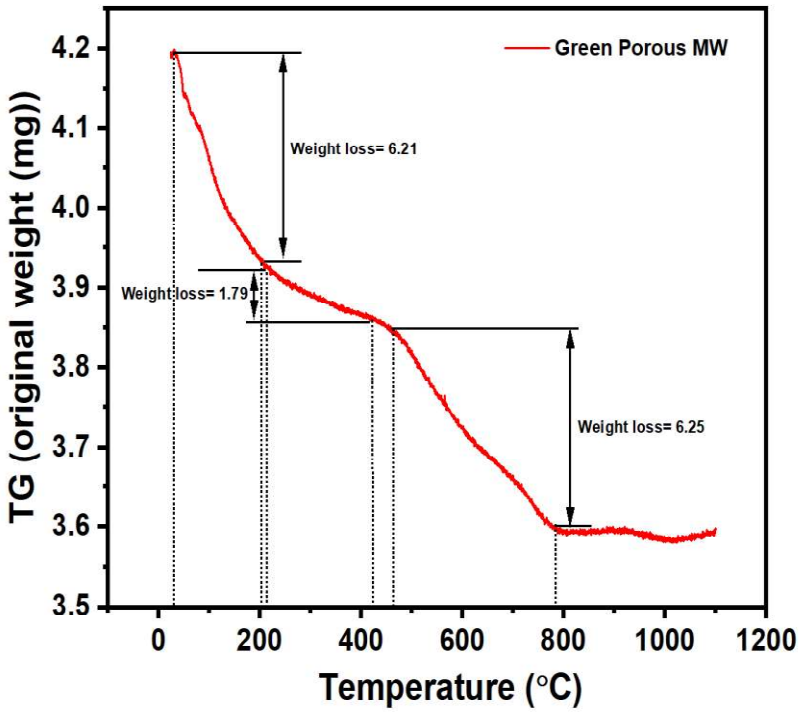

Fig. 5.5 TGA analysis of Green MW composite

Figure 5.6. depicts the Fourier transform infrared (FTIR) spectra of two stages: Green porous MW obtained after alumina dissolution process, and sintered PAC. When the alumina dissolution process starts in MW slurry, various reactions occur concurrently, resulting in the

formation of aluminium hydroxide and aluminium sulphate, as described in the synthesis section. The FTIR spectra of green porous MW support these reaction processes. The analysis reveals changes in the functional groups of the green body, with a strong and broad band centered at 1113 cm^{-1} and 1192 cm^{-1}, attributed to sulphate absorption/SO_4 vibration, confirming the formation of aluminium sulphate which was absent in raw MW. The existence of peaks at 808 cm^{-1} and 918 cm^{-1} due to the stretching vibration of Si-O-Si shows the presence of silicates. The other spectrums observed in the range of 400-550 cm^{-1}, with a small shoulder at 1040 cm^{-1}, corresponds to the Al-O bonds, indicating the coexistence of $Al(OH)_3$ with Al_2O_3. The FTIR spectra suggest that the compounds are hydrates, as evidenced by a broad absorption band around 3600-3700 cm^{-1}, indicating hydroxide stretching vibration, and a band around 1652 cm^{-1} corresponding to the OH bending vibration mode. These findings confirm the presence of both molecular and free water in the samples. The sintered samples exhibit bands at 458 cm^{-1} and 543 cm^{-1}, assigned to Al-O and Al-O-Al vibrations, respectively. The most significant change in functionality compared to the green sample is the reduced intensity of the band associated with the O-H and SO_4 bond, likely due to the evaporation of trapped water and the release of water from $Al(OH)_3$ molecules and removal of sulphates during heat treatment [41, 42, 43]. The existence of peaks at 803 cm^{-1} and 1096 cm^{-1} due to the stretching vibration of Si-O-Si shows the presence of silicates along with alumina compounds at higher temperatures[153].

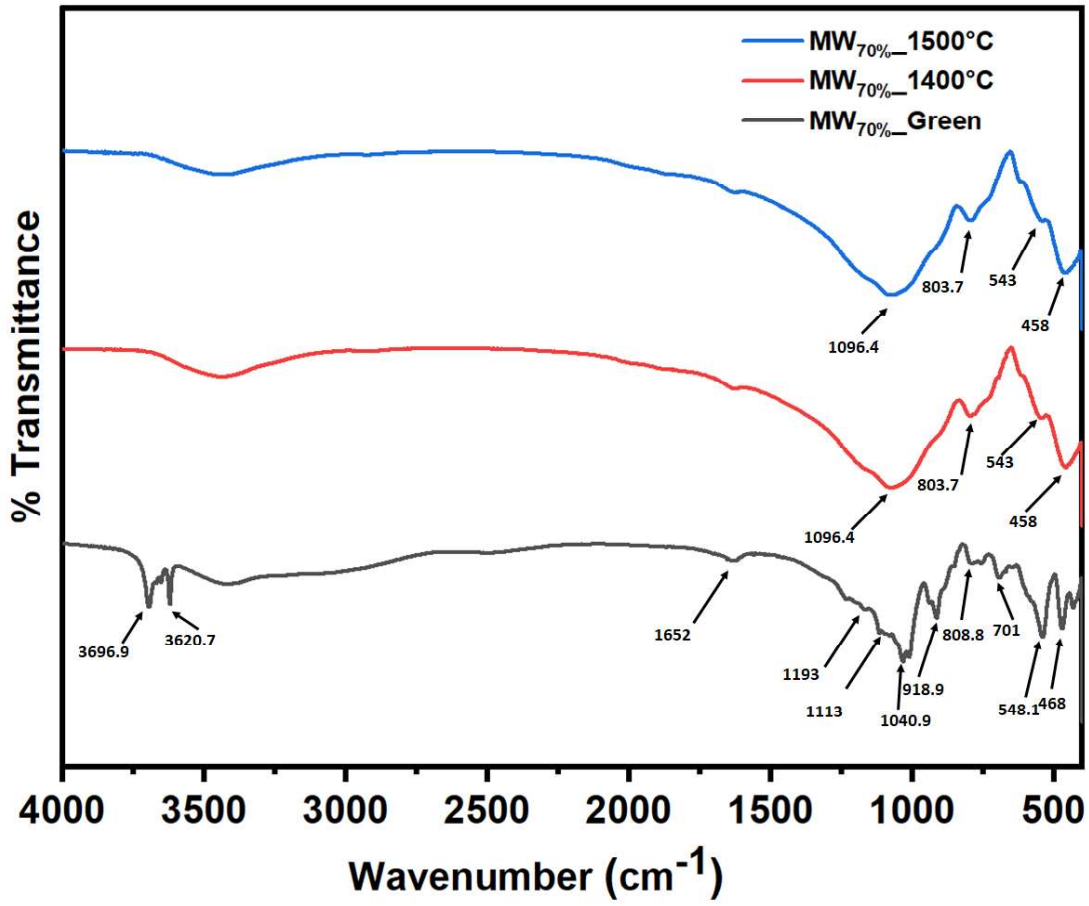

Fig. 5.6 TGA analysis of Green MW composite

The X-ray diffraction (XRD) pattern shown in Fig.5.7 reveals the transformation of various mineralogical phases of the green MW composite during sintering. The mineralogical examination results indicate that most of the aluminosilicate minerals in the raw MW undergo phase transformation and predominantly form the mullite phase [JCPDS No.- 79-1457]. The percentage of mullite phase is higher in samples sintered at 1500°C, indicating better mullitization. The formation of the mullite phase confirms the decomposition of AlOOH and $[Al(OH)_2]_2SO_4$ during heating, which converts to alumina phase and reacts with the silica present in the MW to form mullite. Furthermore, due to the higher content of silicate minerals, silica is the second most abundant compound found in the sintered samples, existing in various forms. The presence of silica as quartz [JCPDS No.- 77-0126] is reduced in the sintered samples due to mullitization, resulting in the transformation of quartz into tridymite [JCPDS No.- 79-1457] and cristobalite phases [JCPDS No.- 82-1233]. The presence of iron sulphide [76-0964], which is considered a significant factor contributing to acid drainage, is reduced or eliminated as a result of the thermal decomposition of iron sulphide and the formation of iron

oxide [JCPDS No.- 84-0309] at higher temperatures. However, the presence of barium sulphide [JCPDS No.- 30-0158] remains a concern for acid drainage issues. Other remaining phases observed at higher temperatures include oxides of sodium (Microcline) [JCPDS No.- 83-1604] and other metal oxides. Complexes of magnesium (Pyrope) [81-0533] and calcium (Titanite) with silicates are also present in small proportions. The formation of these complexes with rare earth elements (REE) and other elements helps in reducing the leaching of these elements.

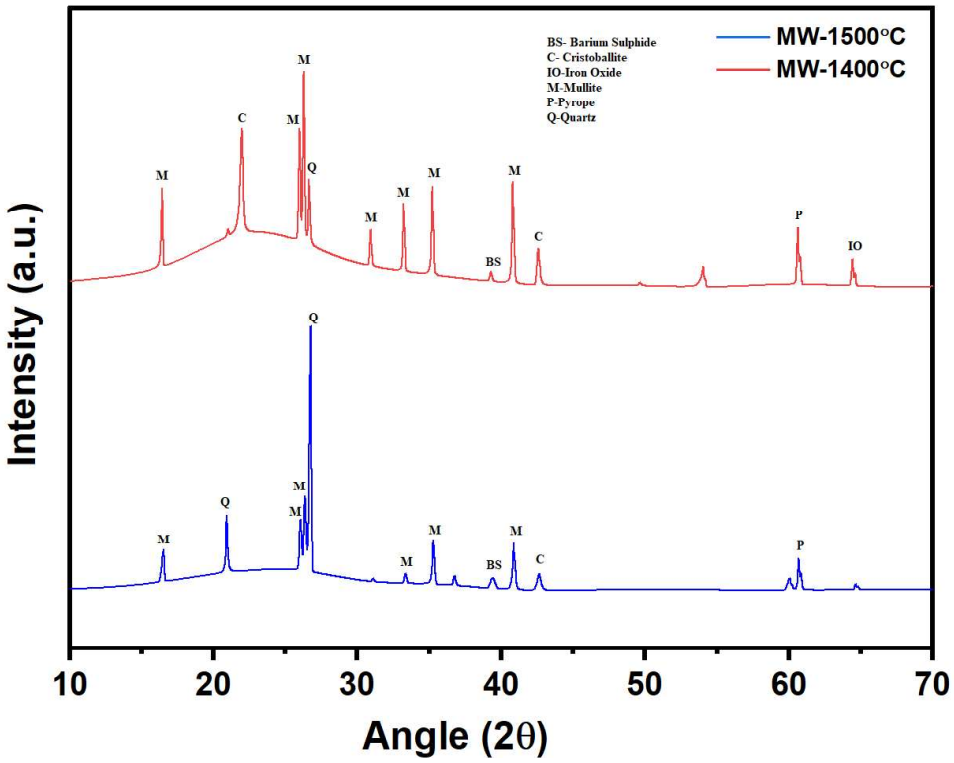

Fig. 5.7 TGA analysis of Green PAC

5.3.3 Optimization of Solid loadings

The slurry loading is identified as the primary factor influencing the porous structure and microstructure of the composite. The optimization of solids loading is based on achieving structural integrity during the drying process of the green porous material. An ideal composition with solids loading is defined as one that results in green samples that possess sufficient strength, uniform shape, and a flat surface without any distortions or defects after initial foaming and drying. It has been observed that very low solids loading, with a minimal amount of solid content, fails to produce green samples with the necessary structural integrity for handling. On the other hand, solids loading that does yield structurally sound green samples is not considered suitable for the production of PAC due to the non-uniform and non-flat surface

characteristics. This relationship is visually depicted in Figure 5.8 (a, c, e), where an increase in solids loading leads to a transition from concave to flat surfaces. A similar effect can also be observed when a higher concentration of sulphuric acid is used. Figure 5.8 (b, d) clearly demonstrates that as the concentration of sulphuric acid increases, the concavity of the surface becomes more pronounced. However, the effect of sulphuric acid diminishes at higher solid content. Through numerous experiments, it has been determined that samples with solids loading ranging from 65% to 80% and 10 wt% sulphuric acid content exhibit desirable results. Therefore, for further analysis and characterization of PAC, three solid loading levels (65%, 70%, and 75%) with 5 wt% sulphuric acid content are considered.

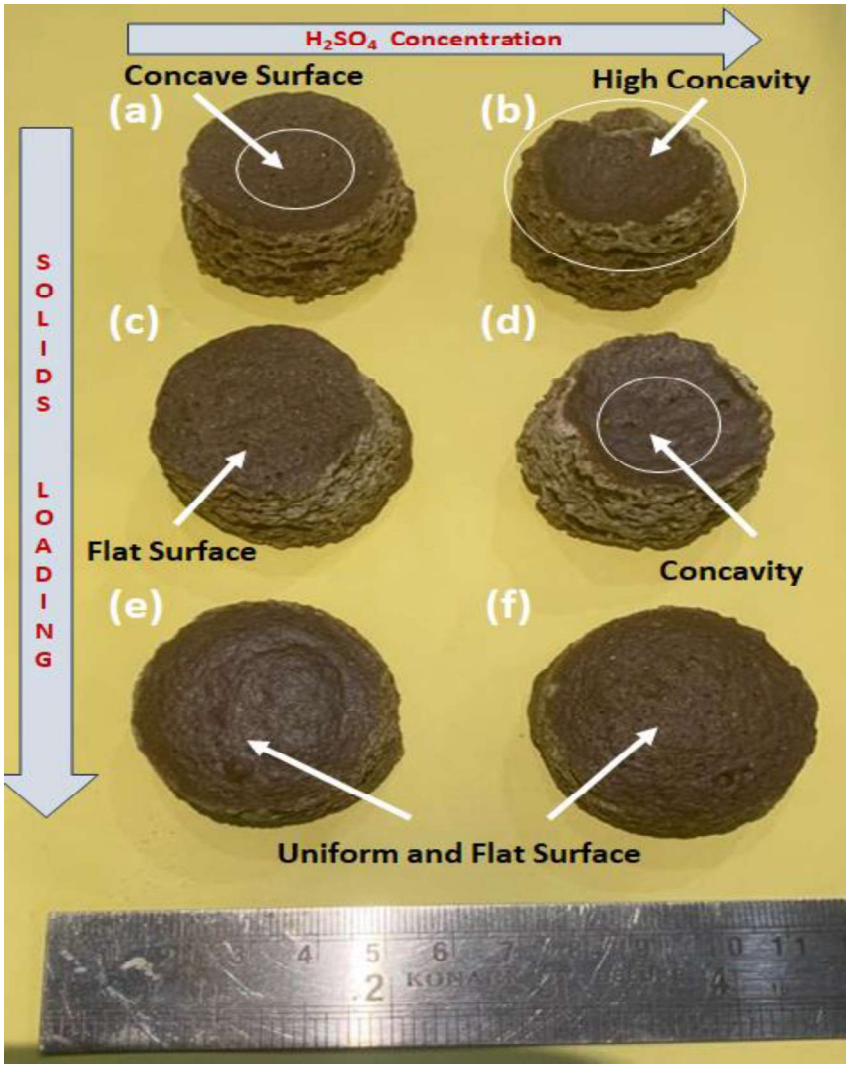

Fig. 5.8 Optical image of PAC prepared with a solids loading of (a) 60 % and 5 wt% H_2SO_4, (b) 60 % and 10 wt% H_2SO_4, (c) 62.5 % and 5 wt% H_2SO_4, (d) 62.5 % and 10 wt% H_2SO_4, (e) 65 % and 5 wt% H_2SO_4, (f) 65 % and 10 wt% H_2SO_4

5.3.4 Microstructural Characterization of Porous Aluminosilicate Composite (PAC)

Fig. 5.9 Optical image of green porous MW composite

As explicitly indicated in the preceding section, achieving an optimized balance between the amount of solids loading and the quantity of sulphuric acid is crucial for maintaining the structural integrity of green MW samples, which enables the support of pores within the resulting porous structure. An exemplification of this green structural integrity can be observed in Figure 5.9, which presents an optical image displaying well-defined pores within a green porous MW sample prepared using 80% solids loading and 10 wt% sulphuric acid. These pores exhibit a distinct and spherical shape. The internal image of the green sample effectively demonstrates the pore morphology, thereby supporting the notion that the bonding of MW particles during foaming is facilitated by the strong binding effect of sulphates. It is anticipated that cells lacking windows will yield closed pores upon sintering, while cells possessing windows will produce open pores in the sintered porous aluminosilicate composite (PAC).

Furthermore, the strength of the porous green MW samples is enhanced through a process of heat treatment and consolidation. Figure 5.10 depicts an optical image of three polished samples in their green and sintered states, each with varying amounts of solids loading. Macroscopic pores present on these samples are clearly discernible to the naked eye. Notably, the size of these macro pores diminishes as the solids content increases, as evident from the images. It is apparent from the image that a higher solid content leads to the formation of more refined pores. This can be attributed to the increased solid content, which hampers the

development of large water bubbles during the foaming process due to the gravitational forces acting on the MW slurry. Another observation gleaned from this image is that the integrity of the pores is maintained during the sintering process, despite the occurrence of secondary pore generation during thermal treatment. The shapes of the pores, as indicated in the image, are largely preserved following sintering (Fig.5.10).

Moreover, to delve deeper into the microstructure of the PAC, SEM micrographs were examined (Fig. 5.11). The findings indicate that the solids loading plays a significant role in shaping the microstructure and pore morphology of the synthesized PAC. The SEM images consistently demonstrate that lower solids loading leads to a higher number of pores, including a greater number of open channels. The elevated total porosity associated with lower solids loadings can be attributed to the increased availability of water in the slurry, facilitating the formation of a greater number of water bubbles and, consequently, generating more pores.

The overall porosity of the samples is influenced by both the number and size of the pores. An increase in the number of pores contributes to higher overall porosity, while larger pore sizes also contribute to increased porosity. Larger pores primarily form due to the presence of water bubbles, while finer pores result from the decomposition of aluminum hydroxides and aluminum sulfates. A slight increase in the number of pores is observed with higher H_2SO_4 concentration, leading to an increase in total porosity.

The stability of pores formed by water bubbles depends on the binding ability of aluminum sulfate. The developed porous composite exhibits a combination of open and closed cells, representing a typical microstructure achieved through the foaming method. The micro-CT image allows for a clear visualization of the porous structure of the sintered PAC material, showcasing the existence of both isolated and interconnected pores (Fig. 5.12). The open pores observed in each sample are relatively large, falling within the macro range or larger. Furthermore, samples with a higher concentration of sulphuric acid exhibit a higher prevalence of open channels. These open pores are the result of water bubbles that rupture during the foaming process, while the closed cells predominantly exhibit a spherical shape.

Fig. 5.10 Optical image of green and sintered PAC.

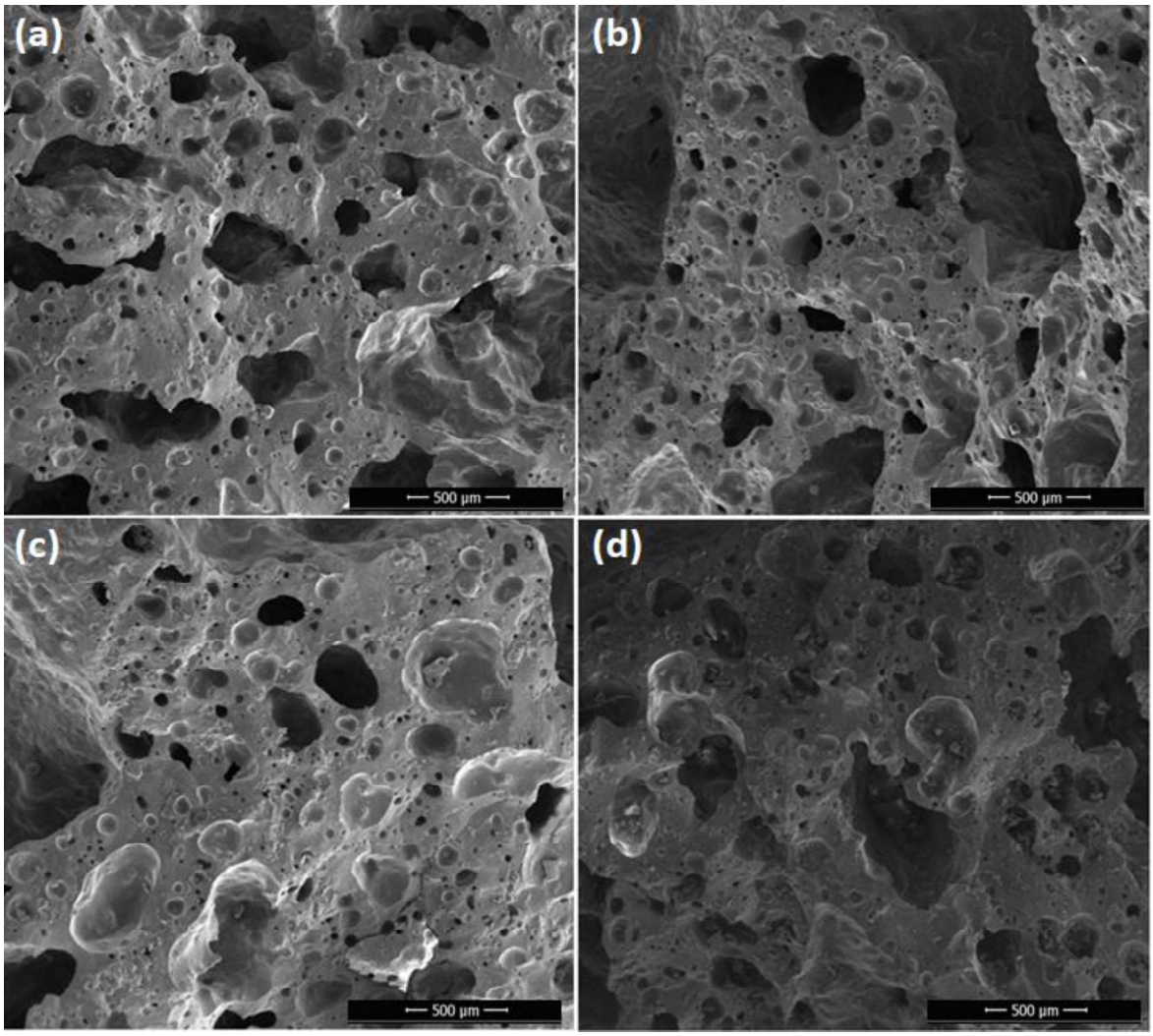

Fig. 5.11 SEM image of PAC (a) 65%-5%- 1400°C (b) 62.5%-5%- 1500°C (c) 65%-10%- 1500°C (d) 77.5%-5%- 1500°C

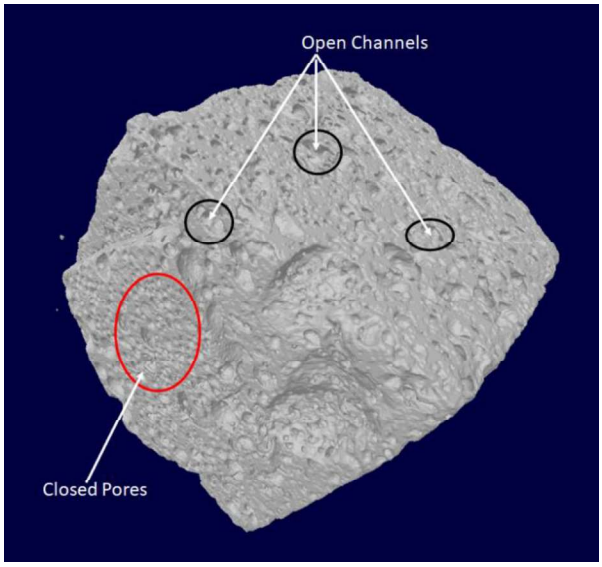

Fig. 5.12 µ-CT image of PAC

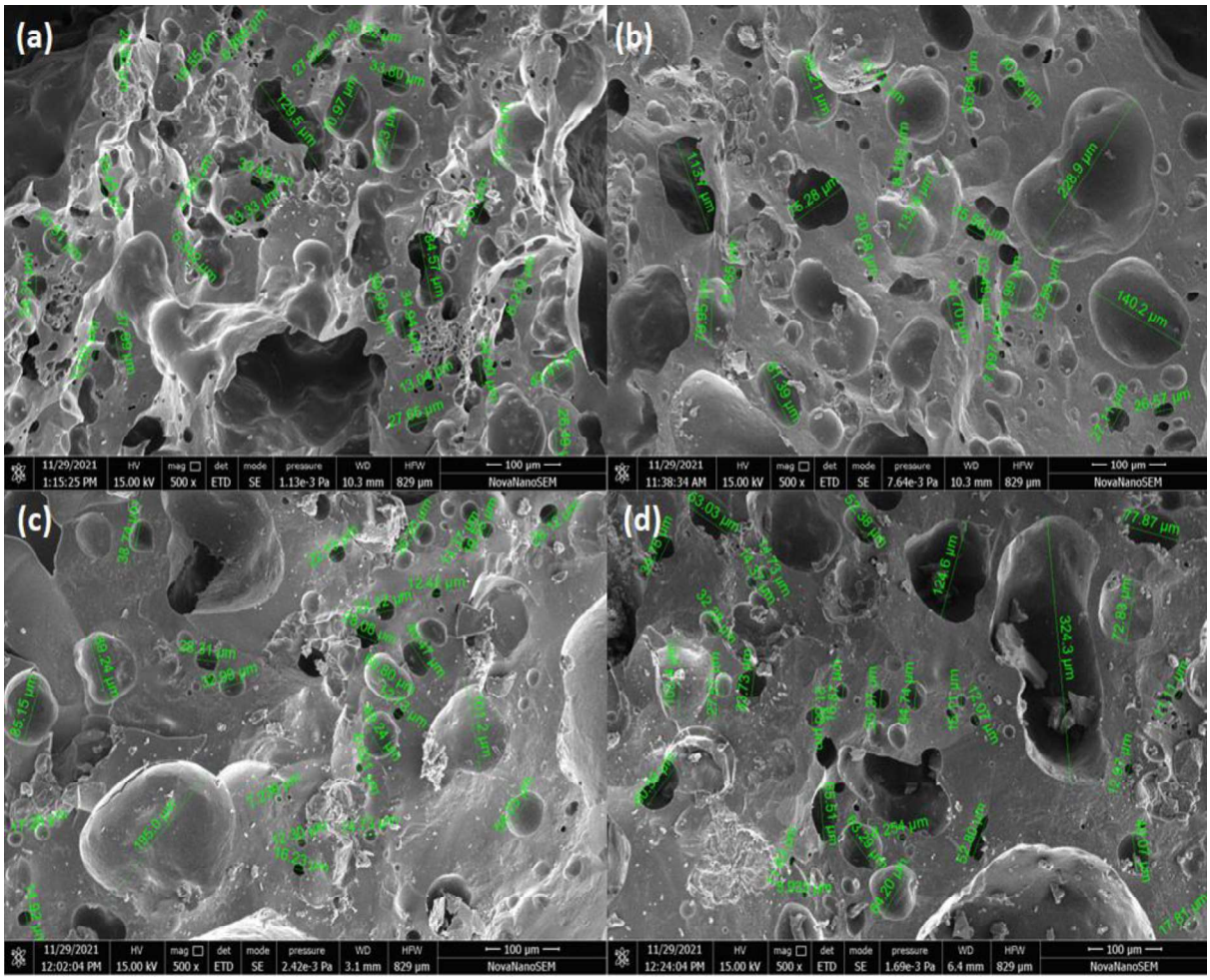

Fig. 5.13 SEM (a) 65%-5%- 1400°C (b) 62.5%-5%- 1500°C (c) 65%-10%- 1500°C (d) 77.5%-5%- 1500°C

Moreover, to examine the influence of solids loading, sulphuric acid content, and sintering temperature on pore size, a detailed microstructural study was conducted using higher magnification SEM images (Fig.5.13). A larger number of pores were observed at lower solids loading, while an increase in pore size was observed with higher solids loading. This variation in pore size with increasing solids loading can be attributed to the formation and stability of larger bubbles. The presence of higher solid contents leads to the formation of thicker and denser struts and bubble surfaces, allowing for the persistence of larger bubbles at higher solids loading. For instance, the average pore size of the PAC prepared with 62.5% solids loading was measured at 38.05 µm, which increased to 44.62 µm when the solids loading was increased to 77.5% (Fig.5.14 (b, d)).

Furthermore, the sintering temperature was found to affect the number of pores, with higher temperatures leading to a decrease in pore quantity due to the increased consolidation rate of

particles. However, the size of pores increased for samples sintered at higher temperatures. This can be attributed to the merging of smaller adjacent pores during consolidation, resulting in the formation of larger pores. For example, the average pore size of the PAC prepared with 62.5% solids loading and sintered at 1400°C was found to be 38.05 µm, which increased to 38.05 µm when the sintering temperature was raised to 1500°C (Figure 5.14 (a, b)). The sulphuric acid content also influenced the pore size, as higher concentrations of H_2SO_4 resulted in a reduction in the average pore size. However, this decrease in pore size was minimal.

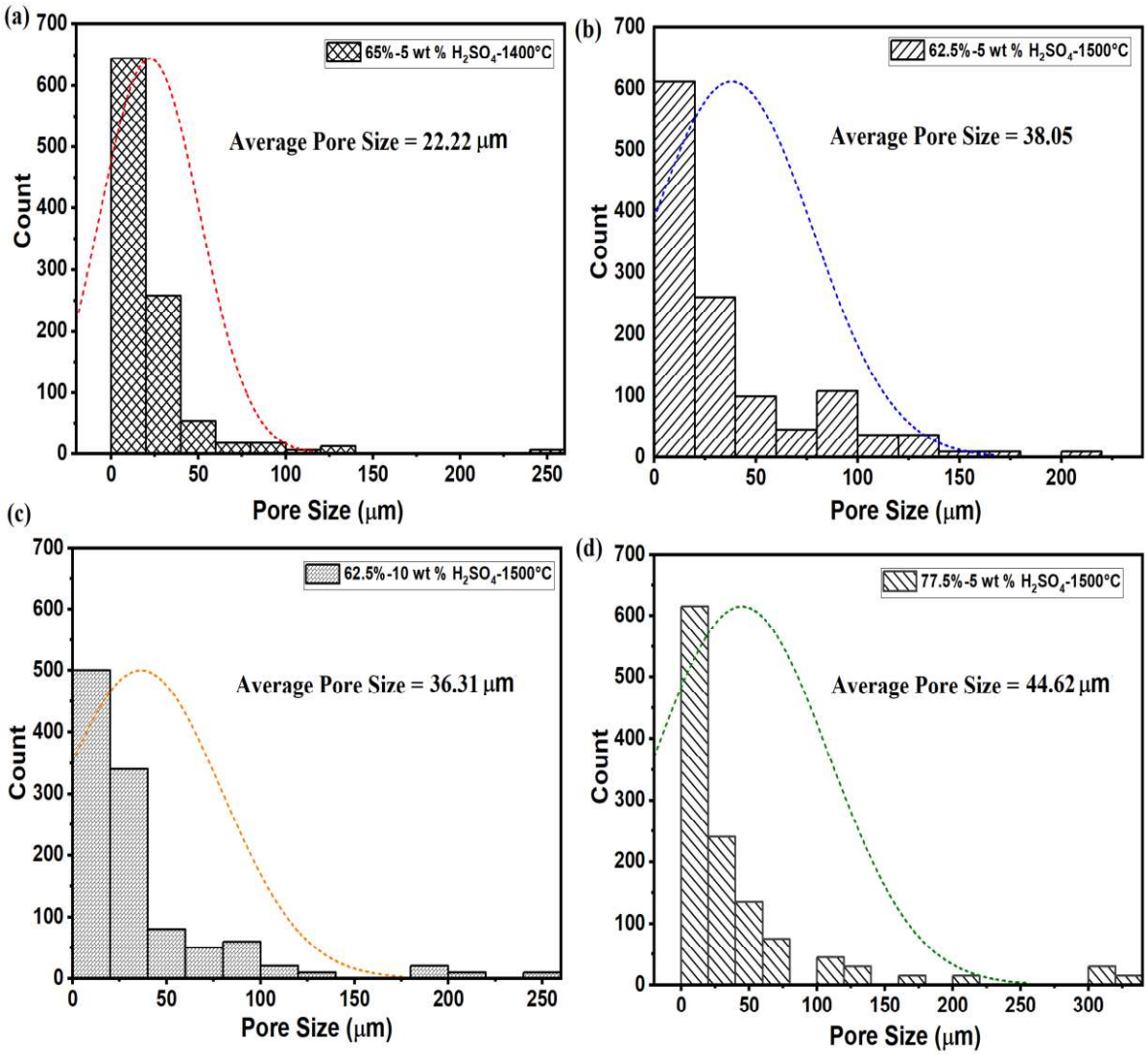

Fig. 5.14 Pore size distribution (a) 65%-5%- 1400°C (b) 62.5%-5%- 1500°C (c) 65%-10%- 1500C (d) 77.5%-5%- 1500°C

In addition to the analysis of macro and micro pores through SEM micrographs, an additional investigation was conducted to examine the presence of nanopores within the structure of the PAC. By closely examining a higher magnified SEM image (Fig 15 (a, b)), it was observed that there were no apparent nanopores between the struts connecting two adjacent pores. This

absence of nanopores can be attributed to the presence of silicate phases, which have a tendency to melt at high temperatures due to the inclusion of oxides such as Ca in the MW composition. These semi-glassy phases effectively fill any existing nanopores that might have existed in the form of inter- or intra-crystallite pores. The SEM image is accompanied by EDS data (Fig.5.15 (c)), which clearly indicates the presence of elements such as Ca, Mg, K, and Fe in smaller proportions, alongside major proportions of Si, Al, and O. These results confirm the formation of dense aluminosilicate phases within the PAC structure.

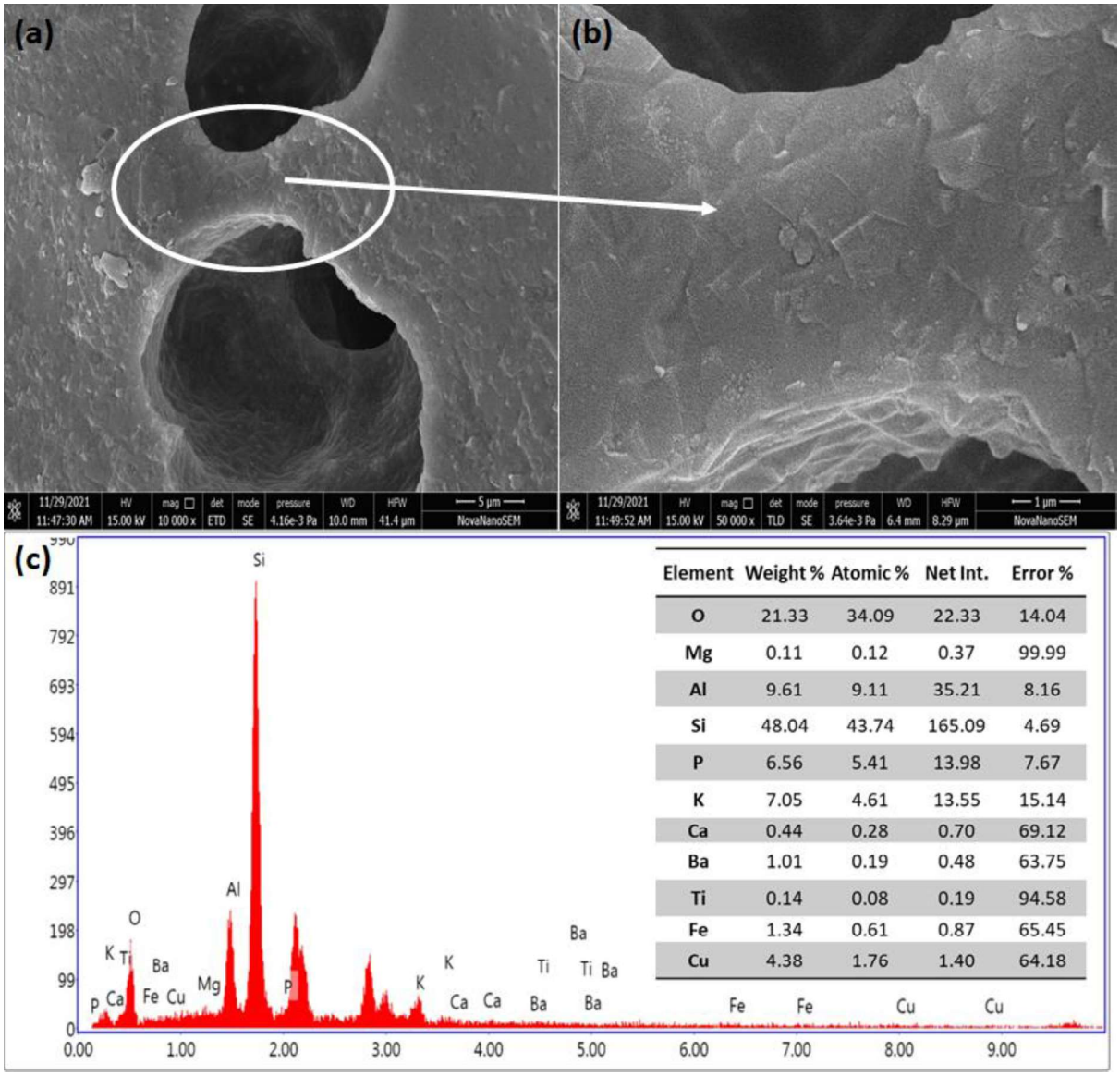

Element	Weight %	Atomic %	Net Int.	Error %
O	21.33	34.09	22.33	14.04
Mg	0.11	0.12	0.37	99.99
Al	9.61	9.11	35.21	8.16
Si	48.04	43.74	165.09	4.69
P	6.56	5.41	13.98	7.67
K	7.05	4.61	13.55	15.14
Ca	0.44	0.28	0.70	69.12
Ba	1.01	0.19	0.48	63.75
Ti	0.14	0.08	0.19	94.58
Fe	1.34	0.61	0.87	65.45
Cu	4.38	1.76	1.40	64.18

Fig. 5.15 (a) SEM showing strut, (b) zoomed view, (c) EDS of PAC

5.3.5 Physical and Thermo-Mechanical Properties of Porous Aluminosilicate Composite (PAC)

Table 5.2Different Mixture Compositions, the Corresponding Microstructural Properties of PAC Fabricated Using Alumina Dissolution Process

Solids Loading	Sintering Temperature (°C)	Bulk Density of (g/cm^3)	Total Porosity (%)	Open Porosity (%)	Closed Porosity (%)	Water Absorption (%)
65	1400°C	1.0009	70.23	24.57	45.66	21.23
70	1400°C	1.00189	67.26	21.34	45.92	18.66
75	1400°C	1.08577	64.52	18.99	45.53	15.67
65	1500°C	1.04095	65.99	12.05	53.94	9.84
70	1500°C	1.05986	64.67	7.64	57.03	6.20
75	1500°C	1.09867	64.1	3.62	60.48	2.9

Table 5.2 summarizes the physical properties of the PAC prepared with different compositions. The PAC exhibits a range of bulk densities (BD) and total porosities, typically ranging from 1 to 1.09 g/cm^3 and 64.1-70.23%. Among the various factors influencing the physical and mechanical properties of the PAC, solids loading and sintering temperature are the most influential. Fig. 5.16 illustrates the variations in BD and linear shrinkage (LS) in relation to solids loading and sintering temperature.

During the sintering process, particle consolidation and grain growth contribute to the overall densification of the material. Two sintering temperatures, 1400°C and 1500°C, have been considered for the consolidation of the porous composite. The samples generally experience shrinkage rather than expansion, resulting in an overall reduction in size after sintering. The LS value tends to be higher at higher sintering temperatures, primarily due to improved grain growth and particle consolidation. Additionally, solids loading significantly influences LS, with lower solids loading leading to greater LS. This can be attributed to a higher rate of densification in samples with lower solid content, as the gaps between particles are more effectively filled. The lowest LS value of 6% is observed for the sample with 75% solids loading sintered at 1400°C, while LS increases to 19% with decreasing solids loading and increasing sintering temperature. Bulk density (BD) is also influenced by solids loading and sintering temperature, with higher values observed at higher temperatures and solids loading.

This is because higher solids loading and sintering temperature promote better packing and densification of the material.

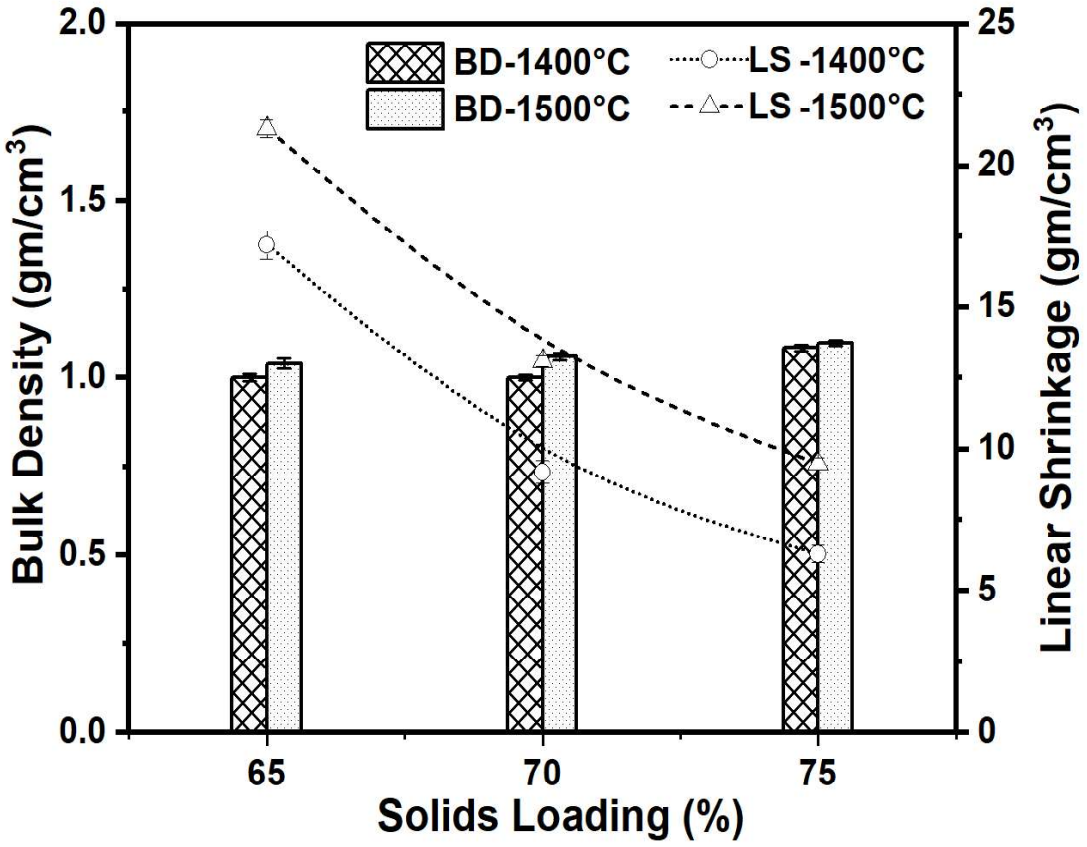

Fig. 5.16 Variations of Bulk Density and Linear shrinkage of PAC with respect to solids loading

The PAC exhibits a total porosity (TP) ranging from 64.1% to 70.23% and a water retention capacity ranging from 2.9% to 21.23%. As the solids loading increases, the TP consistently decreases (Fig. 5.17). This can be attributed to the higher solids loading which restricts the growth of water bubbles, resulting in reduced overall porosity. Similarly, higher sintering temperatures lead to decreased TP due to increased densification, which fills the gaps between particles and reduces porosity.

The water absorption capacity also decreases with increases in solids loading and sintering temperature (Fig. 5.17). A sharp decrease is observed with an increase in solids content. This can be explained by examining the graph of open and closed pores, which clearly indicates a constant decrease in open porosity with increasing solid content (Fig. 5.18). This decrease can be attributed to the presence of larger bubbles and windows at lower solid loadings, which burst and reduce at higher solid loadings. Open and closed porosity exhibit an inverse relationship.

With an increase in solids loading, the number of closed pores increases. This can be attributed to the higher solid contents, which lead to the development of thicker and denser struts and bubble surfaces, enabling the persistence of larger bubbles at higher solids loading. The densely populated solid contents promote the uniform evolution of water bubbles, resulting in consistent pore sizes.

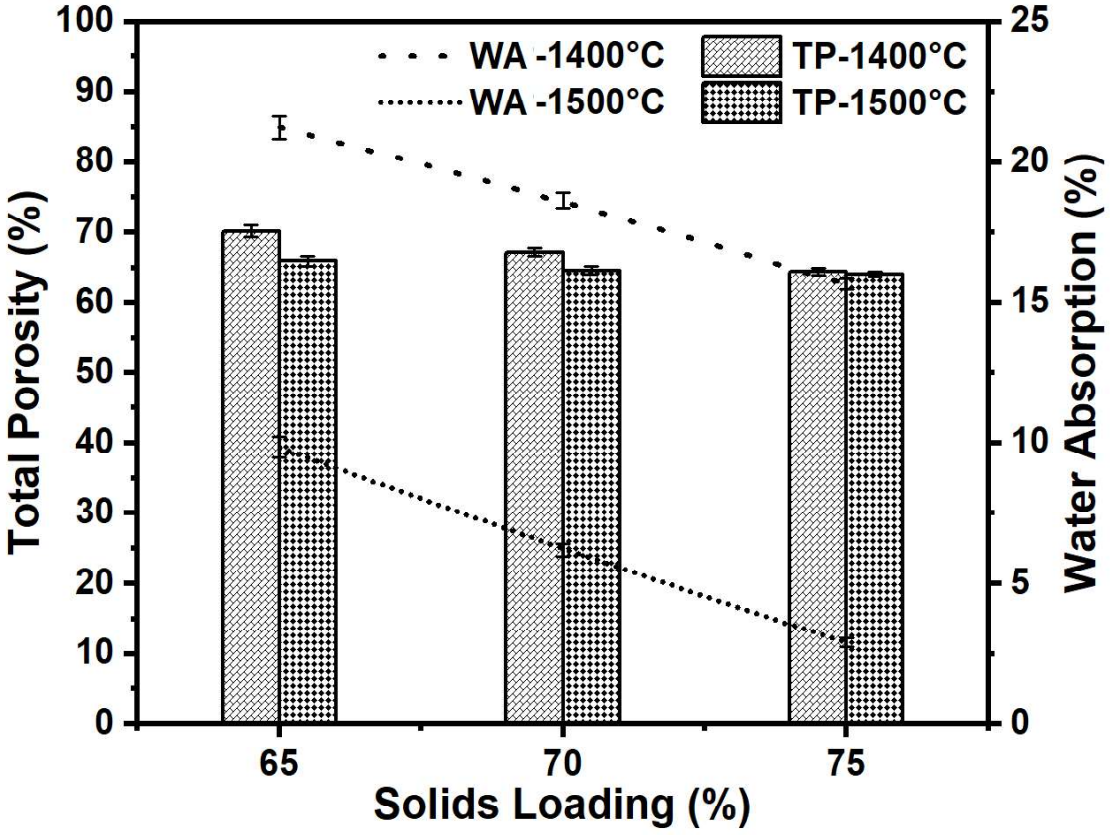

Fig. 5.17 Variations of Total Porosity and Water absorption of PAC with respect to solids loading

The process of sintering at elevated temperatures not only decreases porosity and increases linear shrinkage in the PAC, but it also imparts strength to the structure. Fig. 5.19 depicts the relationship between compressive strength of the PAC, solids loading, and sintering temperature. An increase in solids loading improves compressive strength by reducing porosity, and a higher sintering temperature further enhances the strength of the material. The PAC developed in this study exhibits remarkable compressive strength, ranging from 15.03 to 21.9 MPa.

This exceptional strength can be attributed to the presence of dense and crack-free struts, as observed in Figure 5.15 (a, b), as well as the absence of nano-pores. Additionally, XRD analysis indicates that the mechanical strength of the PAC is enhanced by the formation of aluminosilicate phases, specifically mullite. Mullite possesses a unique structure that imparts superior strength and toughness compared to pure alumina and silica composites. The formation of the mullite phase is facilitated by the high-temperature treatment during sintering, which promotes the reaction between alumina and silica, resulting in the formation of mullite.

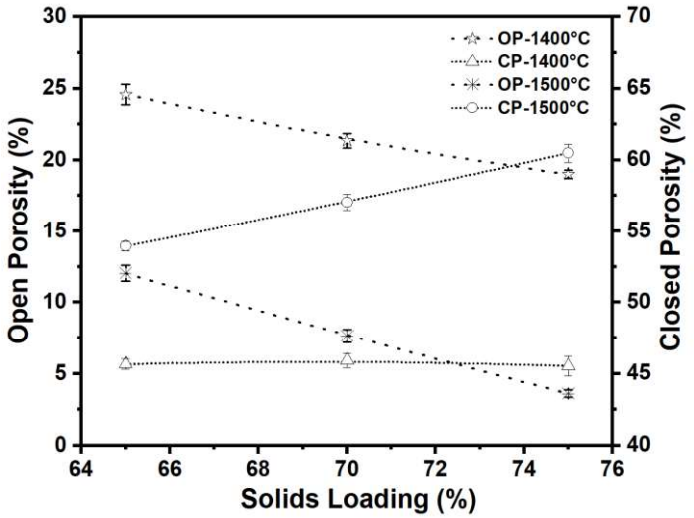

Fig. 5.18 Variations of Open porosity and Closed porosity of PAC with respect to solids loading.

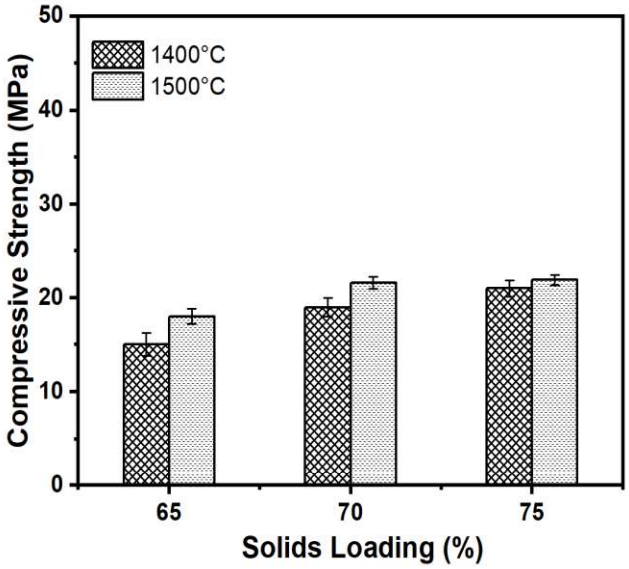

Fig. 5.19 Variations of Compressive strength of PAC with respect to solids loading

5.3.5.1 Thermal Analysis:

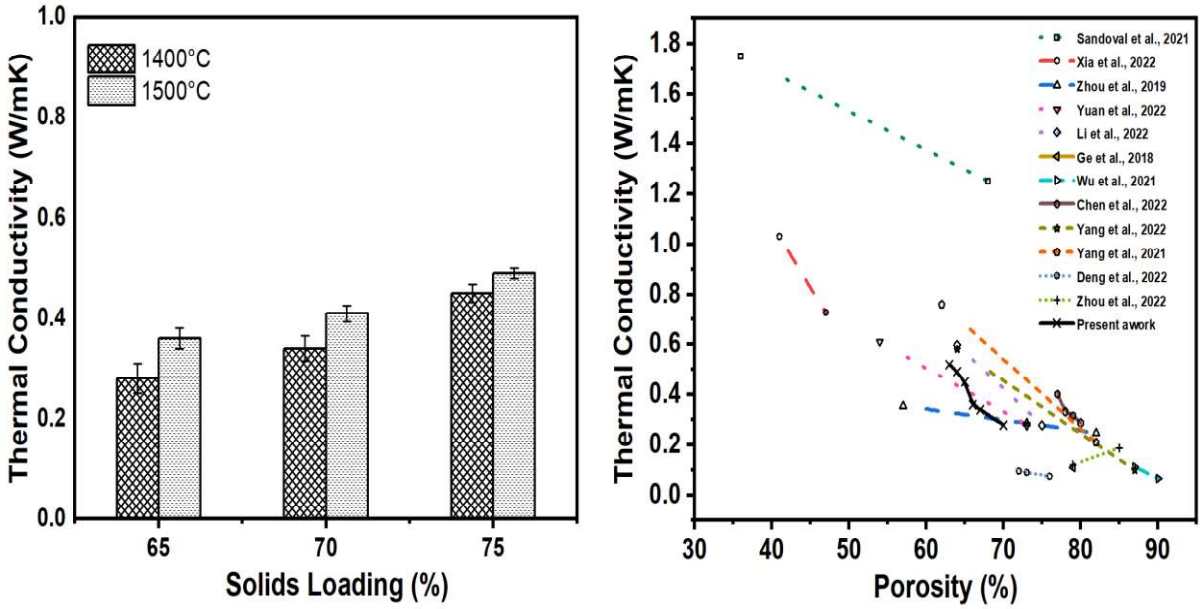

Fig. 5.20 (a) Variations of Thermal conductivity of PAC with respect to solids loading, (b) Comparative chart of TD of PAC with recent reported works

Porous materials are commonly regarded as two-phase systems. In the case of the synthesized PAC, it consists of a solid skeleton and an air phase. The solid skeleton primarily consists of aluminosilicate phases, mainly mullite and silica, as determined from XRD data. To simplify the comparison of data and model-based thermal conductivity calculations, it is assumed that the solid part of the PAC consists of an equal proportion of mullite and silica phases, disregarding other phases present in smaller quantities. The thermal conductivity of the as-fabricated PAC is presented in Fig. 5.20. Surprisingly, the fabricated PAC exhibits a low thermal conductivity of 0.28 W/(m·K), despite mullite and silica themselves possessing high thermal conductivities of approximately 5.2 and 1.5 W/(m·K), respectively. This can be attributed to the relatively lower thermal conductivity of the air trapped within the PAC's pores, which adds extra resistance to heat flow. Notably, the thermal conductivity increases noticeably as the solids loading increases from 65% to 75%. Furthermore, increasing the sintering temperature from 1400°C to 1500°C leads to further enhancement of the thermal conductivity due to decreased porosity. The thermal conductivity data of the developed aluminosilicate samples, obtained through the Alumina dissolution process, is compared with recent studies on porous mullite-based composites. The graph clearly demonstrates that PAC composites exhibit superior thermal resistance compared to most of the recent research on mullite-based porous

composites. Therefore, it can be inferred that the "Alumina dissolution process" has the capability to produce porous composites with excellent thermal resistivity. This can be attributed to the presence of both open and closed cells, where closed cells provide mechanical integrity and open cells offer improved thermal resistivity.

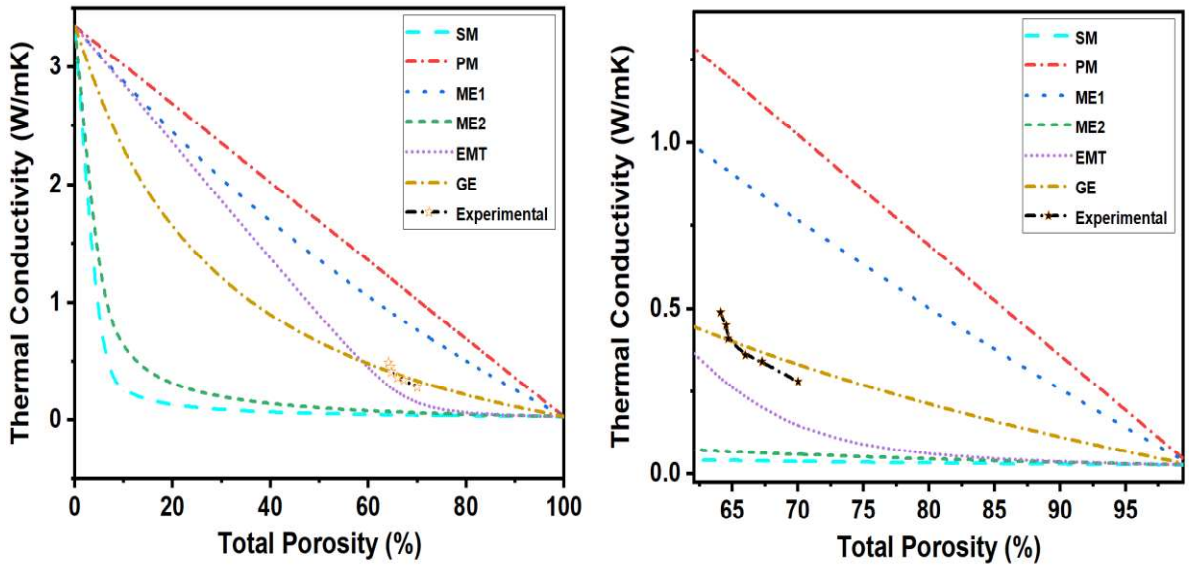

Fig. 5.21 (a) Predicted thermal conductivity of PAC with different models, (b) zoomed view beyond 60%

To better predict the thermal conductivity of porous materials, various models and equations have been developed. Many (if not most) effective thermal conductivity models found in the literature are based on one or more of five basic structural models; specifically, the Series, Parallel, Maxwell–Eucken (two forms) and Effective Medium Theory (EMT) models. However, a heterogeneous material's effective thermal conductivity is strongly affected by its composition and structure, and, as yet, there does not appear to be any single model equation that is applicable to all types of structure. Therefore, the thermal conductivity of PAC having hierarchical pore structures is predicted using the above-mentioned basic models along with Gong equation [154,155] which provides the integrated equation of five basic effective thermal conductivity models (SM, PM, ME1, ME2, and EMT). Thermal conductivity of air, silica and mullite at ambient conditions is considered as 0.026, 1.5 and 5.2 W/(m.K) respectively.

The thermal conductivity of the PAC material was assessed using aforementioned different theoretical models and compared to experimental measurements (Fig. 5.21). To theoretically determine the thermal conductivity of PAC, the solid portion of the PAC was assumed to consist of equal proportions of silica and mullite phases, neglecting other phases, with a thermal

conductivity value of 3.35 W/(m.K). The voids within the PAC were assumed to be filled with air, with a thermal conductivity value of 0.026 W/(m.K). The outcomes obtained from the estimations demonstrate substantial variation in thermal conductivity values across different models. The experimental data does not align with any particular model, but it closely corresponds to the Gong model. Hence, the Gong equation is the most suitable model for predicting and evaluating the thermal conductivity of PAC produced through the alumina dissolution process at ambient temperature.

5.4 Conclusions

The present study aims to address the environmental impact of solid waste containing aluminosilicate minerals by converting it into a valuable product with high-end applications. By utilizing the Alumina dissolution process, a facile, cost-effective, and adaptable approach, highly porous aluminosilicate composites were successfully fabricated. The results demonstrate that this technique enables the production of porous composites with both open and closed pores. The high content of aluminosilicate components in the raw material and the sintering process at elevated temperatures favour the formation of the mullite phase. The fabricated PAC exhibited a range of physical properties, including bulk density, porosity, and compressive strength, with values ranging from 1 to 1.09 g/cm^3, 64.1% to 70.23%, and 15 to 21.99 MPa, respectively. The PAC also exhibited excellent thermal resistivity properties, with low thermal conductivity of up to 0.28 W/(m·K). The developed PAC presents promising industrial applications as filters, thermal insulators, adsorbents, and refractory materials due to their favourable thermoelastic properties. Moreover, the utilization of this process provides a low-cost approach to recycle heterogeneous and hazardous coal mine overburden waste into highly porous ceramic composites. This approach aligns with the principles of circular economy and sustainable development by efficiently recycling aluminosilicate-based industrial waste into mullite-based porous composites.